Bonding in liquid carbon studied by ultrafast x-ray absorption spectroscopy

S. L. Johnson[1], P. A. Heimann[2], A. G. MacPhee[1],

A. M. Lindenberg[1], Z. Chang[3], R. W. Lee[4], and R. W. Falcone[1,5]

[1]*Department of Physics, University of California, Berkeley, CA 94720*

[2]*Advanced Light Source, Lawrence Berkeley National Laboratory, Berkeley, CA 94720*

[3]*Department of Physics, Kansas State University, Manhattan, KS 66506*

[4]*Lawrence Livermore National Laboratory, Livermore, CA 94551*

[5]*Center for Beam Physics, Lawrence Berkeley National Laboratory, Berkeley, CA 94720*

(Dated: February 14, 2003)

Abstract

We employ time-resolved x-ray absorption spectroscopy to the study of femtosecond-laser heated liquid carbon, allowing us to observe the bonding properties at densities near that of the solid. As the density of the liquid increases, we observe a change from predominantly sp-bonded atomic sites to a mixture of sp, sp^2 and sp^3 that compare favorably with tight-binding simulations of the liquid structure at solid densities.

Although considerable attention has focused on solid forms of carbon, the properties of liquid carbon are only vaguely understood. Liquid carbon may exist as a thermodynamically stable phase near the cores of Uranus and Neptune, and it has been hypothesized that it contributes to the measured magnetic moment of these planets [1]. Much of the difficulty for experimental studies of liquid carbon is related to the high temperatures (above 5000 K) and pressures (above 20 MPa) required for thermodynamic stability of the liquid. These conditions are difficult to maintain in long-term equilibrium under laboratory conditions. Consequently, experiments on liquid carbon have had limited success. For example, estimates of the conductivity of liquid carbon in different experiments range from near zero [2, 3] to approximately a factor of ten higher than that of graphite [4]. This variation may be due to a strong dependence of the liquid properties on the temperature and density, but so far no one experiment has made such a relationship clear.

In place of experiments, the work of Wu *et al.* [5] uses first-principles MD simulations as a way to explore the properties of the liquid as function of temperature and density. The calculations show that the local bonding structure of the liquid varies continuously as the pressure increases from the liquid-vapor equilibrium line, with primarily 2-fold coordination at low pressures and densities. The liquid passes through a region of 3-fold average coordination at intermediate densities, and at 3.02 g/cc the simulations show that 4-fold coordination in the melt becomes significant as the average coordination number reaches 3.4. These results are largely consistent with computationally simpler tight-binding simulations at 7000 K [6]. This strong dependence of the local structure on density is an intriguing result that encourages experimental investigation.

To investigate the bonding properties of liquid carbon at near-solid densities, we employed the femtosecond laser pump, x-ray probe technique introduced in ref. [7] to measure the absorption structure at the carbon K-edge immediately after the laser-induced melting of 500 Å thick carbon foil targets. This method, using a synchrotron bend magnet as a broadband source of x-ray probe pulses, offers approximately 70 ps resolution of the melting process and the subsequent expansion dynamics of the liquid.

These expansion dynamics pose an interesting challenge to the experiment. Studies using optical interferometry have estimated the surface expansion velocity resulting from femtosecond ablation in a variety of materials to be as high as 1000 m/s [8]. Assuming this as a maximum expansion rate for 500 Å free-standing carbon foils, we estimate that after 25 ps

the surfaces of the liquid will contain at most twice the initial volume of the foil. This would seem to imply that a time resolution of approximately 5 ps or better is required to probe the liquid carbon at near its initial density, and indeed this is one approach pursued in this report, using an ultrafast x-ray streak camera to resolve the x-ray transmission with this level of temporal resolution. Another approach that avoids many of the problems associated with the experimental complexity of the streak camera is to delay the expansion dynamics of the foil by coating (i.e. "tamping") each side with 3500 Å thick layers of LiF. The large 14 eV optical bandgap of LiF makes this material essentially transparent to the laser, and the mechanical stiffness of the tamping layers prevents the foil from expanding on a time scale $\tau \geq 2d/v \approx 100$ ps, where $d = 3500$ Å is the tamping layer thickness and v is the speed of sound in LiF (approximately 7000 m/s). This expansion delay time τ allows the pump-probe technique (with 70 ps resolution) to observe the liquid at a density near that of the initial solid.

Pump-probe measurements were therefore carried out on three distinct types of solid target foils: (1) 500 Å thick "untamped" films of soft amorphous carbon (sa-C), with a density of 2.2 g/cc (similar to that of graphite), (2) 500 Å thick "tamped" films of sa-C, and (3) 500 Å thick "tamped" films of diamond-like carbon (DLC) with a density of approximately 2.8 g/cc, prepared as described in ref. [9] (without an electrical bias on the substrate). Figures 1 and 2 summarize these measurements of the x-ray absorption near the carbon K-edge. Figure 1 shows the unheated, solid spectrum for each foil, and figure 2 shows the corresponding liquid spectra 100 ps after heating. For the tamped foils, the smooth LiF background absorption has been subtracted out to facilitate comparison with the untamped carbon foil spectra. The liquid spectra all show significant differences from those of the solids, particularly at the narrow pre-edge resonance near 285 eV that is related to the number of π bonded carbon atoms in the material.

The dependence of the observed changes in the spectra as a function of incident laser fluence was checked for each type of foil. In each case, the magnitude of the observed changes reached a saturation level, past which excitation by higher fluences did not further alter the spectra. For the untamped foil, this saturation fluence was 0.7 J/cm^2; for the untamped sa-C and DLC foils, the saturation fluences were both about 2 J/cm^2. The untamped foil fluence data appear to be consistent with similar fluence-dependence measurements of the size of ablation craters left behind by femtosecond laser melting of bulk graphite [10]. Optical self-

absorption measurements using an integrating sphere show that all the foils absorb a similar fraction of the incident intensity (ranging from 40% to 60%), so the difference between the saturation fluence for the untamped and tamped foils may simply be due to thermal diffusion into the tamping layers, which should be significant on the 100 ps time scale of the experiment. The spectra depicted in figure 2 were taken at fluences above this saturation level, suggesting that they do indeed represent the spectra of compeltely melted carbon.

The untamped liquid spectrum did not change measurably with time until approximately 100 ns after melting, when the overall absorption decreases due to hydrodynamic transport of the liquid out of the x-ray probe volume, similar to what was observed for silicon foils [7]. The tamped foils did not appear significantly different from the 100 ps at delays of up to 300 ps, suggesting that the tamping layers successfully confine the liquid to nearly its initial volume on these time scales. At longer times (ca. 100 ns) the tamped foils also showed an overall loss of absorption similar to that observed in the untamped foils.

As a check of the validity of the tamping technique, we also performed the experiment on untamped sa-C foils with an ultrafast x-ray streak camera to obtain 5 ps resolution of the melting process, as described in ref. [7]. Figure 3 shows the spectrum, integrated in time from 5–10 ps after melting, comparing it to the spectrum at 100 ps from the tamped sa-C foils. The spectra are strikingly similar, especially after allowing for the slightly worse spectral resolution obtained with the streak camera.

On a qualitative level, these changes in the spectrum among the different density solids and liquids reflect differences in the local bonding structure in these materials. Specifically, the pre-edge absorption near 285 eV is due to the presence of low-energy bound π^* resonances in the material, a fact that is well established in the literature [11, 13]. The strong increase in absorption at these energies upon melting and with decreasing density thus indicate an increase in the fraction of π bonding in the material. The much broader absorption near 300 eV is from promotion to σ^* continuum states, and so the decrease in absorption near these energies indicates a lower density of the associated types of σ bonds. The liquid data (especially the untamped sa-C liquid) also shows a blue-shift of absorption at these σ^* resonances, an indication of bond length shortening that should be associated with stronger interaction (i.e. more double and/or triple bonding) between carbon atoms.

A quantitative picture of the bonding changes is somewhat complicated by overlap between the π^* and σ^* states, but it nonetheless provides many useful insights. Following a

modified version of the peak-fitting analysis of ref. [11], we attempt to fit the spectra to a sum of absorption features that have been observed and identified in other compounds with carbon-carbon bonding, invoking the so-called "building block" picture. The thin lines under each of the spectra in figures 1 and 2 show the results of this analysis, a decomposition of the spectra into an error-function continuum step and 6 absorption peak. One peak, representing π^* states, was a variable-width Gaussian lineshape fixed in energy at 285.5 eV, approximately the position of the area-weighted average of the two lowest-energy π^* peaks found in ref. [11]. Two more peaks were set to the energy positions and widths of the two lowest-lying σ^* peaks (at 288.5 eV and 290 eV) from ref. [11] that showed no position dependence upon annealing of their solid carbon samples. The three remaining peaks were used to fit the higher energy σ^* continuum resonances. The strong energy-dependence of the width of these continuum resonances motivated the use of the asymmetric Gaussian lineshape from ref. [12] in preference to a simple Gaussian. This lineshape has the form of a Gaussian with an energy-dependent width that varies linearly as $E \times m + b$. With $m = 0.575$ and $b = -164.75$ eV, this lineshape fits accurately a variety of carbon-carbon σ^* resonances above 290 eV for single, double and triple bonds in organic compounds [12]. With these parameters held fixed, the amplitude and energy position of the three high-energy peaks were varied to achieve the best fit. The continuum edge was modeled as a 3 eV wide error function step, held fixed in energy at 289.5 eV, the value obtained in ref. [11] for sa-C. To model the slow drop in absorption as the energy increases far above the edge, the continuum step was multiplied by a linear function of energy that was set to match the observed cross section at 350–450 eV, where all the forms of carbon under study showed nearly identical absorption.

One interesting result of the fits is the movement of the peak positions and change in areas under the three higher energy σ^* resonances. For the solids, ref. [11] assigns the σ_2^* peak near 292 eV to the sum of sp^3 σ^* resonances and conjugated sp^2 bonds from aromatic rings. These conjugated sp^2 bonds also contribute to the σ_4^* peak near 302 eV. The σ_3^* peak near 296 eV is from nonconjugated sp^2 bonds.

These peaks move significantly to higher energies for the fits to the liquid spectra. The presence of sp bonded carbon chains as predicted by ref. [5] should cause the appearance of σ^* resonances at energy positions similar to those observed in organic molecules with sp bonded carbon chains, such as allene, propargyl alchohol, methylacetylene, 2,4-hexadiyne

and acetylene. These spectra have σ^* resonances near 294 eV and 310 eV that are associated with this type of bonding. In allene, these features arise from conjugation between the two C=C σ bonds [13]. In acetylene, only the resonance at 310 eV appears, suggesting that it is due to the short 1.2 Å C≡C bond. Propargyl alchohol, methacetylene, and 2,4-hexadiyne have both resonances, with the lower energy peak from C-C bonds and the higher energy peak from the acetylene-like C≡C bonds. A small additional peak appears at 299 eV in 2,4-hexadiyne, apparently due to a 10% shortening of the central C-C bond by conjugation with the adjacent triple bonds [13]. The large amount of disorder expected in the high temperature liquids under study might also produce spectral features similar the σ^* band of ethylene ($H_2C{=}CH_2$), which is not sp-bonded but does show a strong absorption feature at 300 eV from its unconjugated C=C bond [13].

For all the liquids, the fits place the σ_2^* peak at very near 294.5 eV, a position which agrees remarkably with the lower energy resonances from conjugated C=C σ bonds and unconjugated C-C bonds observed in the sp-bonded molecules discussed above. The σ_4^* resonance moves to values near 312 eV, similar to the higher energy resonance at 310 eV from C=C σ conjugation and C≡C bonds. The σ_3^* component near 300 eV is close to the position of the conjugated C-C bond in 2,4-hexadiyne and the unconjugated C=C bond in ethylene. Of course, the σ_2^* and σ_3^* components of the fit may also contain large contributions from the various resonances that appear in this energy range from the C-C and C=C bonds in sp^3 and sp^2 bonding structures, but the new energy position of σ_4^* appears to be unambiguously due to sp-bonding, be it from conjugation between adjacent C=C bonds or from C≡C bonds.

Although the peak positions show little dependence on the liquid density, the area under the σ_4^* peak does show a very significant difference between the untamped and tamped liquids. Since this peak serves as an indicator of sp-bonding in the liquid, the fact that the untamped, low-density liquid shows more absorption from this feature does suggest a higher fraction of sp-bonded carbon than in the more dense liquids. The area under this absorption feature in the high density liquids (normalizing to the total area of the spectrum) is approximately 75% of the area under this peak in the untamped liquid.

To estimate the number of π bonds relative to the number of σ bonds in the liquids, we rely on an application of the important Thomas-Reiche-Kuhn sum rule. This rule states that the sum of the oscillator strengths for a given electron in an atom or molecule to all other states is unity. Assuming that the total p-projected density of unoccupied states is

also constant, this implies that the total area under the K-edge spectrum is the same for all the different forms of structurally disordered carbon under study [11]. Indeed, the total spectral area integrated from 275–400 eV was observed to be approximately constant, within 4%.

Provided that the sum rule holds and the oscillator strength of all π^* resonances is constant (see appendix), we can estimate the relative numbers of π^* states in each form of carbon by taking the area under the π^* peaks and normalizing by the total area under the spectrum. Table I summarizes the results.

The quoted errors in the π^* area are based on the idea that the primary source of error is in the mistaken assignment of oscillator strength near 288–290 eV, the region of the spectrum where the π^* and σ^* resonances overlap. The lower bound of the error in the π^* area is set to the integral of the fitted π^* peak over energies above 288.5 eV, the peak position of the lowest σ^* resonance. Similarly, the upper bound of the error is set to the sum of the areas under the sigma resonances and the continuum step for energies below 288.5 eV. This method sometimes gives very asymmetric error ranges (especially in the case of the untamped liquid), but it provides a reasonable estimate of the actual error in the absorption from π^* states for the liquids. For the solids these errors are probably exaggerated, since the higher quality data of ref. [11] does a good job of identifying resonances in this energy range.

Inspection of the results for the two solids in table I shows a nearly 60% higher level of π^* contributions in the soft a-C than in the DLC. This agrees with the measurements of ref. [11] that estimate 70% of the sites in their soft a-C samples are sp^2 bonded and 40% of the sites in their DLC samples are sp^2 bonded.[14] Since each sp^2 site contributes one π^* state to the spectrum and sp^3 sites contribute no π^* states, we can make quantitative statements about the average number of π^* states per site if we assume that the soft a-C foils used in the pump-probe experiments are indeed 70% sp^2. These estimates are listed for each form of carbon in table I, giving a reasonable value of 45% for the sp^2 fraction of the DLC foils. This level of quantitative agreement with other measurements of the π^* bond fraction is an important check of the analysis.

For the liquids there is much more π bonding evident from the fits. The low-density untamped liquid shows nearly 3 times the number of π^* states than does the soft a-C solid. From the rightmost column in table I, we estimate that each site in the untamped liquid

contributes an average of 2.01 π^* states to the absorption spectrum in agreement with the 2 states/atom expected for purely sp hybridized bonding. For the tamped liquids, we can compare the data quantitatively to the results of the $T = 7000$ K tight-binding simulations of ref. [6]. Values for the π^* states/atom in the simulations are listed in the rightmost column of table I. Agreement between the simulation and fit results is good for the 2.2 g/cc liquid, with both estimating about 1.3 π^* states/atom. At 2.8 g/cc the simulation and fits still agree within the estimated errors, but whereas the simulation predicts fewer π^* states/atom compared to the 2.2 g/cc liquid, the fits do not show a significant change with density.

Although this methodology of fitting the pump-probe spectra of liquid carbon to overlapping resonances is somewhat limited by the noise level of the experimental data, it is largely successful in providing an experimental measure of the bonding properties in the liquid at various densities near that of the solid. At low densities, the low density liquid is predominantly sp bonded. At higher densities attained by tamping the heated foils the fraction of sp bonded sites is still significant, and the estimated number of π^* antibonding states/atom agrees with the results of published simulations of the liquid structure based on a tight-binding interaction model.

APPENDIX: OSCILLATOR STRENGTH OF π^* RESONANCES

Let $|\psi\rangle$ be a particular π^* state in an amorphous solid or liquid carbon. Under the LCAO (linear combination of atomic orbitals) scheme, this state can be written as a superposition of the atomic $|2p\rangle$ orbitals over the different carbon sites [13]:

$$|\psi\rangle = \sum_j \left(a_j \left|2p_z\right\rangle_j + b_j \left|2p_x\right\rangle_j + c_j \left|2p_y\right\rangle_j \right). \tag{1}$$

Imposing the normalization condition $\left|\langle\psi|\psi\rangle\right|^2 = 1$ and assuming no significant overlap between the orbitals of different sites,[15] we obtain

$$\sum_j \left(|a_j|^2 + |b_j|^2 + |c_j|^2 \right) = 1. \tag{2}$$

Since the electronic states are (in aggregate) orientationally disordered, we may further simplify this as

$$\sum_k \left(|a_j|^2 \right) = 1/3. \tag{3}$$

Now consider x-ray absorption from the localized 1s core states within the material to $|\psi\rangle$. The oscillator strength f_k for absorption from a particular site k is

$$f_k = \frac{2}{mE} \left| \langle \psi | \, \mathbf{e} \cdot \mathbf{p} \, | 1s \rangle_k \right|^2 = \frac{2mE}{\hbar^2} \left| \mathbf{e} \cdot \langle \psi | \, \mathbf{r} \, | 1s \rangle_k \right|^2 . \tag{4}$$

Let us define the z-axis of the atomic orbitals to be the polarization direction $\mathbf{e}$ of the x-rays. We can then write

$$f_k = \frac{2mE}{\hbar^2} \left| \langle \psi | \, z \, | 1s \rangle_k \right|^2 . \tag{5}$$

Since the 1s core state is highly localized, in evaluating the matrix element $\langle \psi | \, z \, | 1s \rangle_k$ for a given absorber we can ignore contributions to $|\psi\rangle$ from the atomic orbitals of other sites. We can then evaluate the matrix element by integrating in position space to obtain

$$\langle \psi | \, z \, | 1s \rangle_k = \frac{4\pi R}{3} a_k^* \tag{6}$$

where $R = \int_0^\infty R_{1s}(r) R_{2p}(r) r^3 \mathrm{d}r$, and the functions $R_{1s}(r)$ and $R_{2p}(r)$ are radial components of the atomic wavefunctions [13]. The *total* oscillator strength f_{tot} for all possible transitions to $|\psi\rangle$ is then

$$f_{\mathrm{tot}} = \sum_k f_k = \frac{32mE}{9\hbar^2} |R|^2 \sum_k |a_k|^2 = \frac{32mE}{27\hbar^2} |R|^2, \tag{7}$$

where the last step invokes the state normalization condition of equation 3. Since f_{tot} is independent of the coefficients a_k, b_k and c_k that compose the final state $|\psi\rangle$, it is the same for all such states. Each π^* state thus contributes equally to the area under the absorption cross section.

The Advanced Light Source is supported by the Director, Office of Science, Office of Basic Energy Sciences, Materials Sciences Division, of the U.S. Department of Energy under Contract No. DE-AC03-76SF00098 at Lawrence Berkeley National Laboratory.

[1] M. Ross, Nature **292**, 435 (1981).

[2] A. Ludwig, Zeit. Elektrochem. **8**, 273 (1902).

[3] M. T. Jones, *Nat. Carbon Res Lab. Report PRG* (1958).

[4] J. Heremans, C. H. Olk, G. L. Ecsly, J. Steinbeck, and G. Dresselhaus, Phys. Rev. Lett. **60**, 452 (1988).

[5] C. J. Wu, J. N. Glosli, G. Galli, and F. H. Ree, Phys. Rev. Lett. **89**, 135701 (2002).

[6] J. R. Morris, C. Z. Wang, and K. M. Ho, Phys. Rev. B **52**, 4138 (1995).

[7] S. L. Johnson, P. A. Heimann, A. M. Lindenberg, H. O. Jeschke, M. E. Garcia, Z. Chang, R. W. Lee, J. J. Rehr, and R. W. Falcone (2003).

[8] K. Sokolowski-Tinten, J. Bialkowski, A. Cavalleri, and D. von der Linde, Phys. Rev. Lett. **81**, 224 (1998).

[9] S. Anders, A. Anders, I. G. Brown, B. Wei, K. Komvopoulos, J. W. A. III, and K. M. Yu, Surf. Coat. Technol. **68/69**, 388 (1994).

[10] D. H. Reitze, H. Ahn, and M. C. Downer, Phys. Rev. B **45**, 2677 (1992).

[11] J. Díaz, S. Anders, X. Zhou, E. J. Moler, S. A. Kellar, and Z. Hussain, Phys. Rev. B pp. 125204/1–19 (2001).

[12] D. A. Outka and J. Stöhr, J. Chem. Phys. pp. 3539–54 (1988).

[13] J. Stör, *NEXAFS Spectroscopy* (Springer-Verlag, Berlin Heidelberg, 1992).

[14] The fraction was 40% for freshly deposited DLC films, increasing to nearly 60% after annealing.

[15] This "zero overlap assumption" is reasonably accurate for π bonding. It is used successfully in the perturbative Hückel theory to obtain the splitting of π and π^* orbitals in hydrocarbons [13].

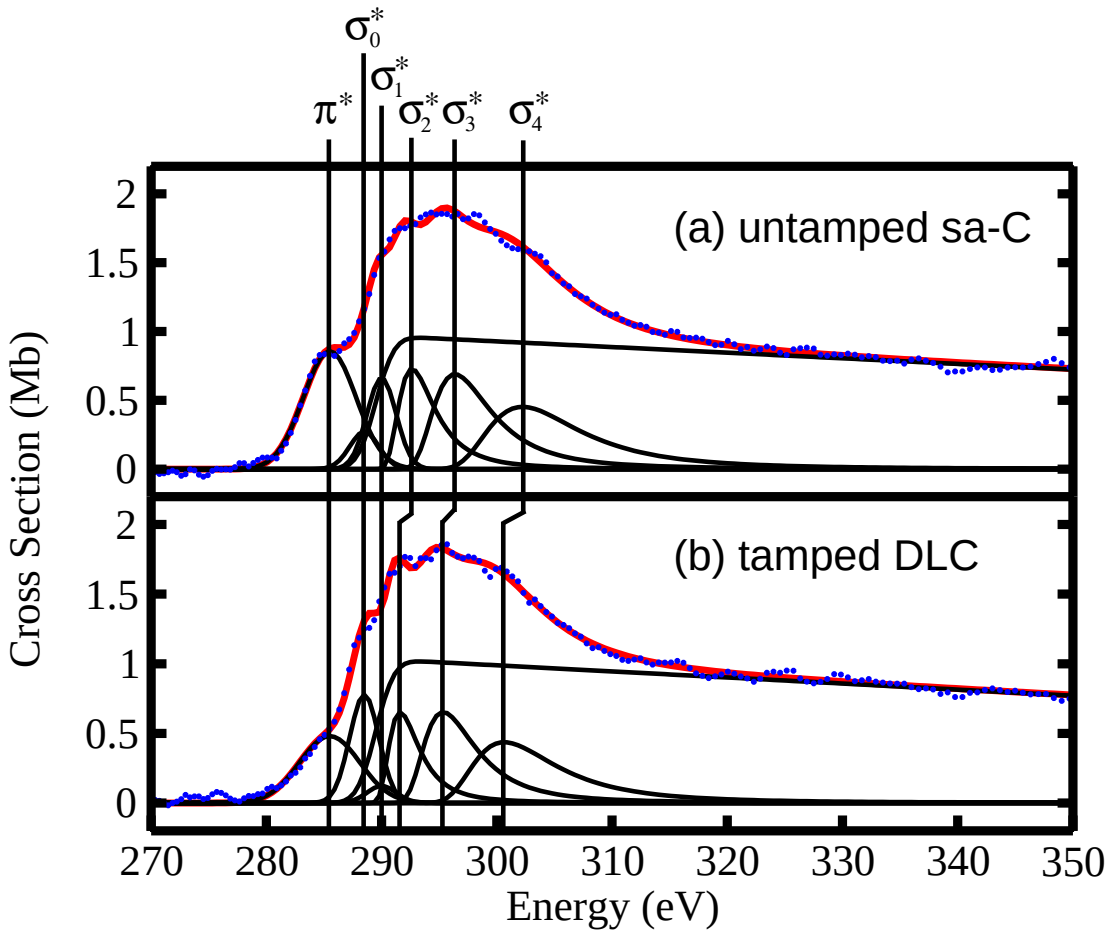

FIG. 1: K-edge absorption spectra of unheated carbon foils: (a) sa-C (untamped), and (b) tamped DLC, after subtracting out the LiF absorption. These data are taken with the same statistics as the heated spectra of figure 2. The tamped sa-C spectrum (after subtracting out the LiF contributions) looks very similar to (a), but with a larger noise level due to the 80% signal loss from the tamping layers.

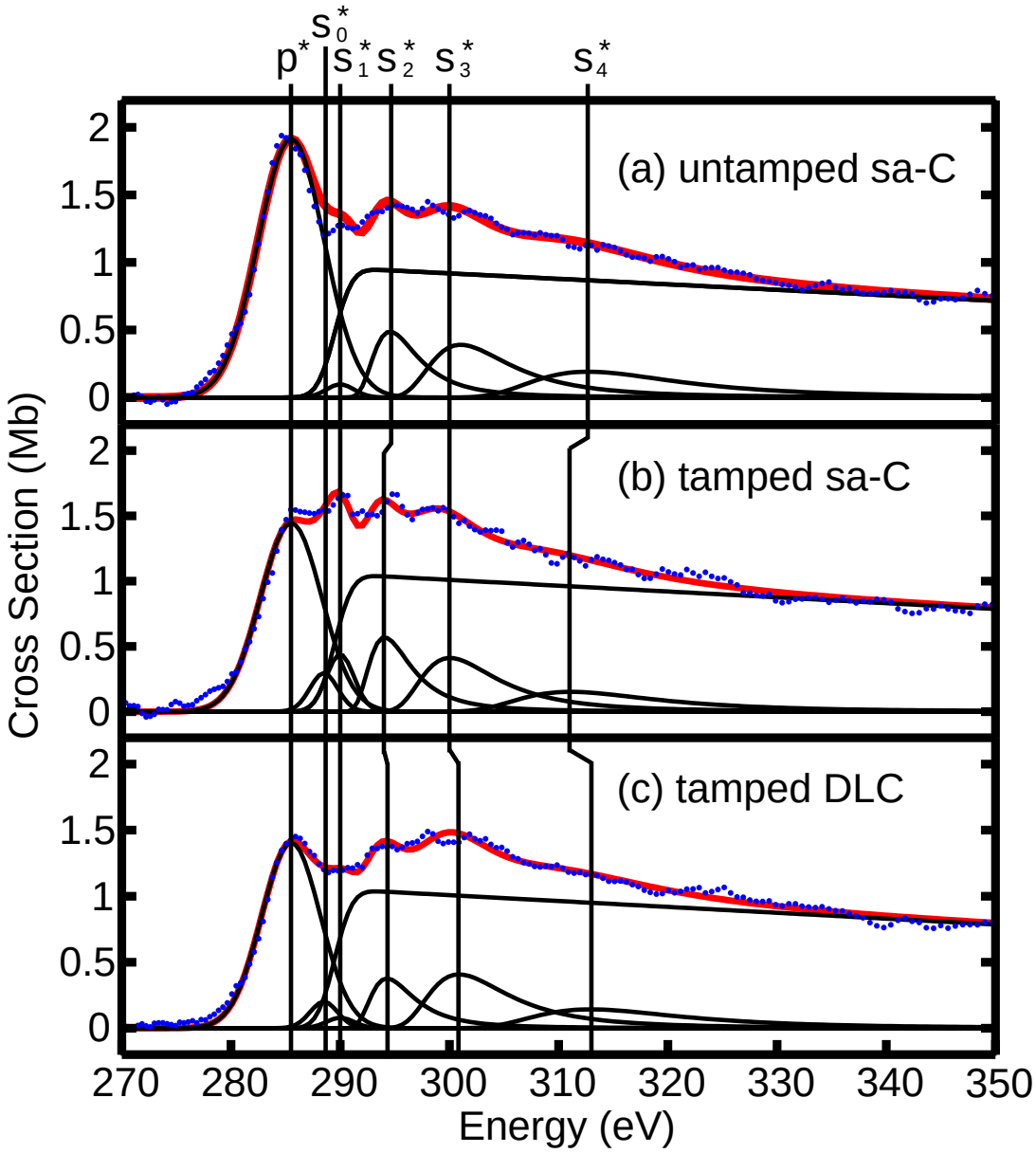

FIG. 2: K-edge absorption spectra of carbon foils 100 ps after heating: (a) sa-C (untamped), (b) tamped sa-C, and (c) tamped DLC. For the tamped foils, the LiF background absorption has been subtracted out.

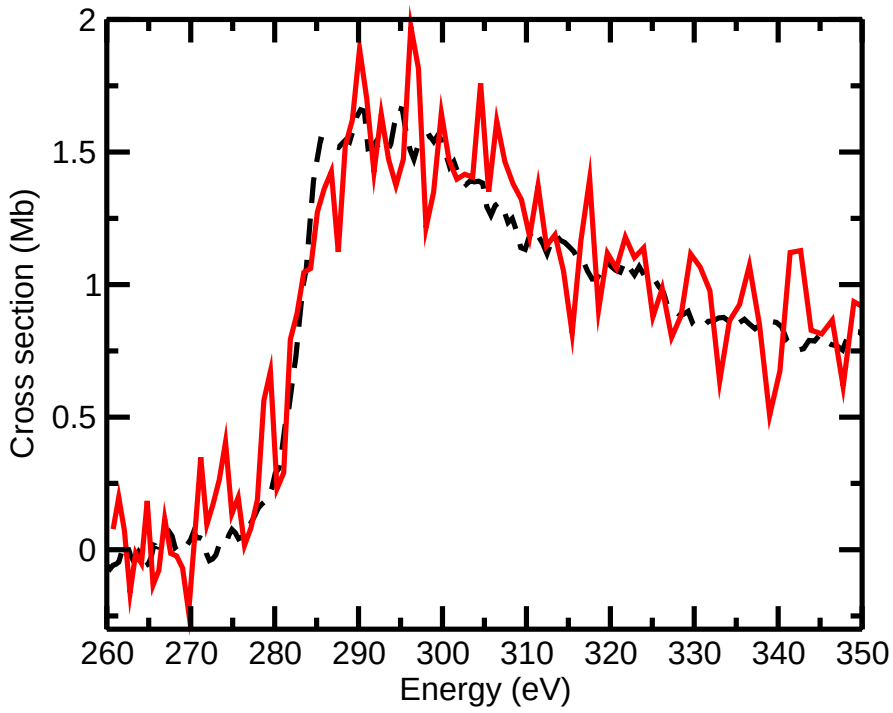

FIG. 3: Solid line: absorption spectrum from heated sa-C obtained using the streak camera detector, integrating in time from 5–10 ps after excitation. Dashed line: tamped sa-C spectrum from figure 2b.

material	π^* area	π^* states/site	π^* states/site (ref. [6])
soft a-C	$0.047^{+0.008}_{-0.004}$	$0.70^{+0.12}_{-0.06}$	-
DLC	$0.030^{+0.014}_{-0.004}$	$0.45^{+0.20}_{-0.06}$	-
untamped liquid	$0.135^{+0.002}_{-0.020}$	$2.01^{+0.03}_{-0.30}$	-
2.2 g/cc liquid	$0.090^{+0.007}_{-0.013}$	$1.35^{+0.10}_{-0.20}$	1.29 ± 0.04
2.8 g/cc liquid	$0.087^{+0.005}_{-0.011}$	$1.29^{+0.07}_{-0.20}$	1.05 ± 0.12

TABLE I: Relative contribution of π^* states to the absorption spectra of solid and liquid forms of carbon, as derived from the fits. The table also lists estimates of the number of π^* states per site, assuming a most likely value of 0.70 for the soft a-C solid. The rightmost column lists the π^* states/site derived from the simulation results in ref. [6]. The errors in these values are based on the estimated uncertainty in the density of the target carbon ($\pm 5\%$ for sa-C and $\pm 7\%$ for the DLC).